

Universal fluctuations of Floquet topological invariants at low frequencies

M. Rodriguez-Vega¹ and B. Seradjeh^{1,2}

¹*Department of Physics, Indiana University, Bloomington, Indiana 47405, USA*

²*Max Planck Institute for the Physics of Complex Systems, Nöthnitzer Str. 38, 01187 Dresden Germany*

We study the low-frequency dynamics of periodically driven one-dimensional systems hosting Floquet topological phases. We show, both analytically and numerically, in the low frequency limit $\Omega \rightarrow 0$, the topological invariants of a chirally-symmetric driven system exhibit universal fluctuations. While the topological invariants in this limit nearly vanish on average over a small range of frequencies, we find that they follow a universal Gaussian distribution with a width that scales as $1/\sqrt{\Omega}$. We explain this scaling based on a diffusive structure of the winding numbers of the Floquet-Bloch evolution operator at low frequency. We also find that the maximum quasienergy gap remains finite and scales as Ω^2 . Thus, we argue that the adiabatic limit of a Floquet topological insulator is highly structured, with universal fluctuations persisting down to very low frequencies.

The behavior of a periodically driven system can be qualitatively different from its equilibrium behavior. Manifestations of such behavior in classical physics include resonances, dynamical stabilization of new steady states, and the period-doubling approach to chaos [1–3]. In quantum systems, the effective Floquet dynamics of a driven systems has been employed as a powerful way to engineer designer Hamiltonians, e.g. by using laser sequences in cold atomic gases. In this way, novel phases of matter have been proposed and realized [4–8].

More recently, it has been understood that a driven system can also exhibit essentially non-equilibrium *topological* phases, dubbed Floquet topological phases [9–12]. Drive parameters, such as the frequency Ω or the shape of the drive (“drive protocol”) have been proposed [13–21] and used in the lab [22–25] to engineer a rich array of topological phases not possible in equilibrium systems. The non-equilibrium dynamics at large frequencies is relatively well understood, e.g. within rotating-wave approximation, as a renormalization of the equilibrium parameters of the system [26–30]. The low-frequency regime, on the other hand, remains largely unexplored [32]. This is the relevant regime in solid-state systems driven by ac potentials [11]. It is also important as a way to reduce unwanted heating in the system [33–36]. At a more basic level, it relates to the adiabatic limit as $\Omega \rightarrow 0$. Numerical studies have reported nonzero Floquet topological invariants as frequency is lowered [15, 37–41]. This raises questions on the nature of adiabatic limit in Floquet topological phases.

In this paper, we study the low-frequency limit of one-dimensional model driven systems that exhibit a rich Floquet topological phase diagram [12, 15]. Assuming the driven systems are chirally symmetric [1, 41, 43], we derive analytical expressions for the Floquet topological invariants and evaluate them numerically over several decades of the drive frequency. We find that these topological invariants not only remain nonzero at low frequencies, but increasingly fluctuate. While at any fixed frequency the invariants are deterministic, over a range of frequencies $\delta\Omega \ll \Omega$, the invariants distribute pseudo-

randomly. We argue that this distribution is universal and in our models is given by a Gaussian, whose width is $\sigma(\Omega) \sim 1/\sqrt{\Omega}$. We explain this universal behavior by revealing a diffusive process in the evaluation of the invariants and confirm our results numerically.

Specifically, we study one-dimensional driven systems with periodic boundary conditions, with a Hamiltonian of the form $\hat{H} = \int \hat{c}_k^\dagger h_k \hat{c}_k \frac{dk}{2\pi}$, where $k \in [-\pi, \pi]$ is the crystal momentum, \hat{c}_k is a two-component spinor field, and $h_k = d_{kx}\sigma_x + d_{ky}\sigma_y$ with $d_{kx} + id_{ky} \equiv d_k$ a model-dependent function. For example, in the Su-Schrieffer-Heeger (SSH) model [44, 45] $d_k = 2e^{ik/2}(w \cos \frac{k}{2} + i\delta \sin \frac{k}{2})$, where w (δ) is the hopping (modulation) amplitude. In the Kitaev model [45, 46], after a suitable rotation in the Nambu space, one finds $d_k = 2w \cos k - \mu + i\Delta \sin k$, where μ is the chemical potential and Δ is the nearest-neighbor pairing amplitude.

These Hamiltonians are particle-hole symmetric, $\sigma_z h_k^* \sigma_z = -h_k$, with eigenvalues $\pm |d_k|$. In equilibrium, there are two topologically distinct phases: a topological phase, for $\delta/w > 0$ in the SSH and $|\mu| < 2|w|$ for Kitaev model, and a trivial phase otherwise. These two phases are distinguished on the lattice with open boundary conditions by the presence of zero-energy bound states in the topological phase. With periodic boundary conditions, the phases are distinguished by an integer topological invariant $\nu = 0$ or 1, equal to the winding number

$$\nu = \mathcal{W}[d] \equiv \frac{1}{2\pi i} \int_{-\pi}^{\pi} \frac{\partial}{\partial k} \ln(d_k) dk. \quad (1)$$

For a multi-band system, e.g. the SSH-Kitaev [45, 47], d_k is matrix-valued and the topological invariant is found by $\mathcal{W}[\det d]$.

When the system is periodically driven, the full dynamics is obtained by solving the Floquet-Schrödinger equation $[h_k(t) - i\partial_t]\phi_k^\pm(t) = \pm \epsilon_k \phi_k^\pm(t)$ (we are setting $\hbar = 1$) for the periodic steady states $\phi_k^s(t) = \phi_k^s(t + 2\pi/\Omega)$, $s = \pm$, with the quasienergy $s\epsilon_k$, which we take to be in the Floquet zone $[-\Omega/2, \Omega/2]$. The Bloch evolution operator can then be written as $U_k(t) =$

$\sum_{s=\pm} e^{-is\epsilon_k t} \phi_k^s(t) \phi_k^{s\dagger}(0)$. The full-period evolution operator $U_k(2\pi/\Omega)$ has eigenstates $\phi_k^s(0)$ with eigenvalues $e^{-2s\pi i \epsilon_k/\Omega}$. Since the quasienergy is a modular quantity, even a two-band model is characterized by two gaps at Floquet zone center ($\epsilon^b = 0$) and Floquet zone edge ($\epsilon^b = \Omega/2$) [48]. Thus, for periodic boundary conditions there are *two* independent topological invariants defined for the quasienergy gaps at Floquet zone center, ν^b , and edge, ν^b . For open boundary conditions, the corresponding invariants are the number of midgap steady bound states at Floquet zone center and edge [45].

To simplify our discussion, we take the drive protocol to satisfy the chiral reflection symmetry, $\delta(t + \pi/\Omega) = \delta(-t + \pi/\Omega)$; then, the two topological invariants are found [1, 45] from the half-period evolution operator $U_k(\pi/\Omega) \equiv \begin{pmatrix} A_k & B_k \\ C_k & D_k \end{pmatrix}$, as

$$\nu^b = \mathcal{W}[B] \quad \text{and} \quad \nu^b = \mathcal{W}[D]. \quad (2)$$

In the static case, D_k is constant and $B_k \propto d_k$, thus one finds $\nu^b = 0$ and $\nu^b = \nu$ as expected. For concreteness, we present our results for the SSH model in the following and for other models in the Supplemental Material [45].

At symmetry points $k_s = 0, \pm\pi$, $h_{k_s} \propto \sigma_x$ and the half-period evolution operator takes simple forms, $U_0(\pi/\Omega) = e^{-i\frac{2\pi}{\Omega} w \sigma_x}$ and $U_\pi(\pi/\Omega) = e^{i\frac{2\pi}{\Omega} \delta \sigma_x}$, where $\bar{\delta} = (\Omega/2\pi) \int_0^{2\pi/\Omega} \delta(s) ds$ is the average hopping modulation through one drive cycle. The values $D_{\pm\pi} = \cos(2\pi\bar{\delta}/\Omega)$, $D_0 = \cos(2\pi w/\Omega)$ and $B_{\pm\pi} = i \sin(2\pi\bar{\delta}/\Omega)$, $B_0 = -i \sin(2\pi w/\Omega)$ can be used to anchor their winding.

To understand the changes in the winding number ν^b (ν^b) we analyze the contour of D_k (B_k) in the complex plane as frequency varies (see Fig. 1). At high enough frequency the contour of D_k (B_k) is a loop with two crossing points on the real (imaginary) axis at $D_{\pm\pi}$ and D_0 ($B_{\pm\pi}$ and B_0); as frequency is lowered the loop twists and untwists, thus changing the number of crossing points on the real (imaginary) axis via two processes: a pair of crossings are “emitted” from D_0 (B_0) whenever $D'_0 = 0$ ($B'_0 = 0$), where the prime denotes $\partial/\partial k$; on the other hand, a pair of crossings are “absorbed” into $D_{\pm\pi}$ ($B_{\pm\pi}$) when $D'_{\pm\pi} = 0$ ($B'_{\pm\pi} = 0$). While the rates of these processes depend on the drive protocol, they all scale with $1/\Omega$; thus the number of crossings generically grows as $1/\Omega$. As Ω is lowered, all crossings *move* back and forth within the unit disk along the real (imaginary) axis at a speed that scales with $1/\Omega$. When a crossing point of D_k (B_k) passes through the origin, the winding ν^b (ν^b) changes. The inversion symmetry of the SSH model ensures that except $D_{\pm\pi}$ and D_0 ($B_{\pm\pi}$ and B_0), all other crossings are doubled.

Denoting the momenta at crossing points with $k_c^\circ(\Omega)$, where $\circ = b, b$, the total number of crossings is $N^\circ = N_+^\circ + N_-^\circ$, where $N_\pm^\circ = \sum_c \Theta(\pm D_{k_c^\circ} \text{Im } D'_{k_c^\circ})$ and $N_\pm^b = \sum_c \Theta(\pm i B_{k_c^b} \text{Re } B'_{k_c^b})$. The winding numbers, on the

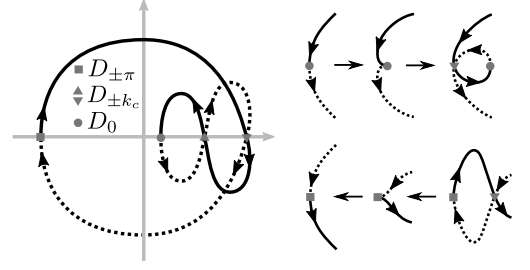


FIG. 1. The topological invariant ν^b is the winding number of the complex function D_k , $k \in [-\pi, \pi]$ (left), computed from the crossing points on the real axis. The inversion symmetry of the SSH model yields a reflection symmetric contour around the real axis, the solid (dashed) line designating the portion corresponding to $k \in [-\pi, 0]$ ($[0, \pi]$). As the frequency is lowered, new crossing points are emitted from D_0 when the contour twists (top right) and absorbed into $D_{\pm\pi}$ when it untwists (bottom right).

other hand, are given by $\nu^\circ = \frac{1}{2}(N_+^\circ - N_-^\circ)$. At any given frequency, Ω , the values of N_\pm° may be computed deterministically from the number of crossings emitted, absorbed, and moved on the corresponding real or imaginary axis. However, as $\Omega \rightarrow 0$, these numbers grow in an increasingly complex way; thus, over a frequency interval $\delta\Omega \ll \Omega$ the distribution of crossing points appears random. We posit that this distribution can be modeled by a universal stochastic process of emission, absorption, and motion of crossing points of D_k (B_k) [49]. In the low-frequency limit, our numerics show generically that N_\pm° are equally distributed. Taking this to be true, we may think of N_\pm° as the number of steps taken by a one-dimensional random walker in opposite directions, with $2\nu^\circ$ the distance from the starting point. Thus, winding numbers are diffusive variables with a protocol-dependent diffusion constant $\mathcal{D}^\circ = 2\Omega\sqrt{\langle N_+^{\circ 2} \rangle}$. Here, $\langle \dots \rangle$ stands for the average in the stochastic model or, equivalently, the average over the interval $\delta\Omega$. The winding numbers acquire a Gaussian distribution with a width $\sigma^\circ(\Omega) = \sqrt{\mathcal{D}^\circ/\Omega}$. This is our main result.

Changes in the winding number are concomitant with quasienergy gap closings. This is easy to see at symmetry points k_s , where, for our chirally symmetric protocols, the full-period evolution operator is the square of the half-period evolution operator. At these points, ν^b (ν^b) change by one when D_0 and $D_{\pm\pi}$ (B_0 and $B_{\pm\pi}$) vanish, respectively, at $\Omega_0^b = \frac{4w}{2m-1}$ and $\Omega_\pi^b = \frac{4\bar{\delta}}{2m-1}$ ($\Omega_0^b = \frac{2w}{m}$ and $\Omega_\pi^b = \frac{2\bar{\delta}}{m}$) for integer m . Noting that quasienergies at symmetry points are given by $\epsilon_0 \equiv \pm 2w \bmod \Omega$ and $\epsilon_\pi \equiv \pm 2\bar{\delta} \bmod \Omega$, it is easy to see they are equal to ϵ^b (ϵ^b) exactly at frequencies where ν^b (ν^b) changes. Of course, changes in ν^b (ν^b) are also caused at any frequency Ω_*^b (Ω_*^b) and non-symmetry momenta $k_*^b \equiv k_c^b(\Omega_*^b)$ [$k_*^b \equiv k_c^b(\Omega_*^b)$], where $D_{k_*^b}$ ($B_{k_*^b}$) vanishes and the gap at ϵ^b (ϵ^b) closes. Due to inversion symmetry, the winding numbers at these gap closings change by two. We note that the

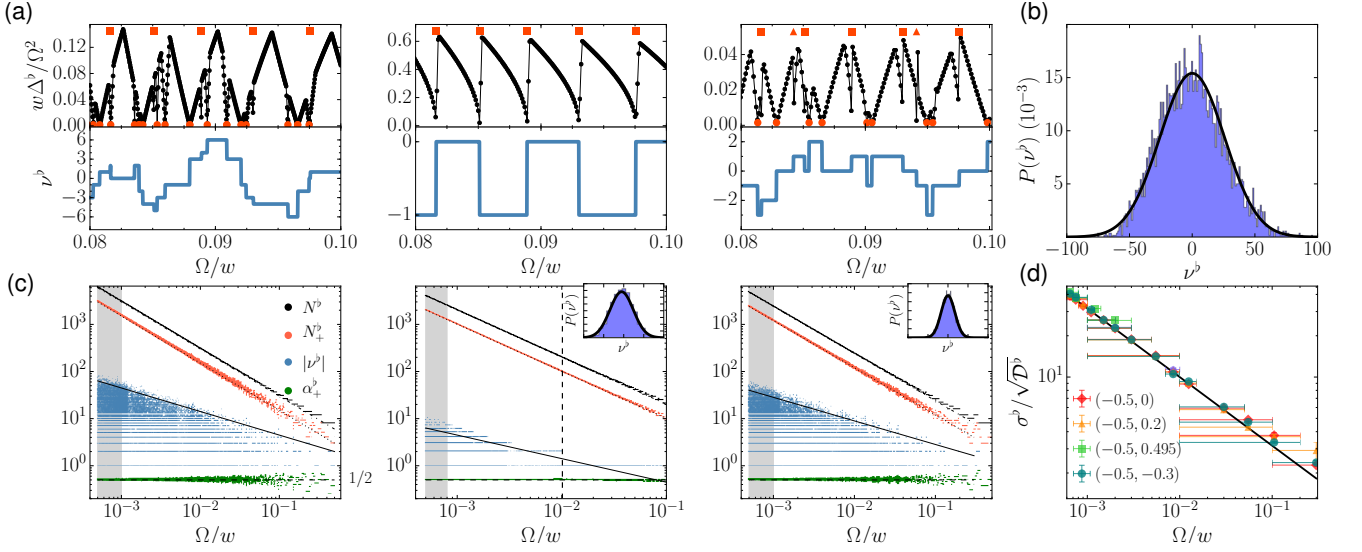


FIG. 2. (color online) (a) The quasienergy gap (top panels) and the topological invariant (bottom panels) at the Floquet zone edge as a function of the frequency. The two-step drive protocols are critical ($\delta_1/w = -0.5, \delta_2/w = 0$, left), asymmetric ($\delta_1/w = -0.5, \delta_2/w = 0.495$, center), and trivial ($\delta_1/w = -0.5, \delta_2/w = -0.3$, right). In all cases $p_1 = p_2 = 0.5$. The (orange) markers indicate analytically calculated gap closings at the symmetric points $k_s = 0$ (square), and $k_s = \pm\pi$ (triangle) and non-symmetric points $k_c^\circ \neq k_s$ (circle). (b) Probability distribution of ν^b for the critical protocol in (a) and frequency range $\Omega/w \in (0.5, 1) \times 10^{-3}$. The solid line is a Gaussian fit. (c) Statistics of crossing points and winding number for the three drive protocols in (a). From top to bottom in each panel: the total number of crossing points, N^b , the positively-oriented crossing points N_+^b , the ratio $\alpha_+^b = N_+^b/N^b$, and the winding number $|\nu^b|$ are calculated numerically at 65000 frequencies. At this resolution, fluctuations in the winding numbers render their graphs random. The vertical dashed line in the center panel marks twice the value of the asymmetry parameter. The insets show the probability distribution $P(\nu^b)$ over the shaded range as in (b). The solid line shows $\sqrt{D^b/\Omega}$ with $D^b = ||\delta_1| - |\delta_2||$. (d) Standard deviation $\sigma^b(\Omega)$ for various two-step drive protocols found by a Gaussian fit to $P(\nu^b)$. The horizontal (vertical) line at each point indicates the range of frequencies (fitting error). The legend shows the values $(\delta_1/w, \delta_2/w)$. The solid line is $\sigma^b = \sqrt{D^b/\Omega}$.

frequencies Ω_*^b and Ω_*^{\natural} depend on the drive protocol.

To proceed quantitatively, we choose a periodic two-step drive protocol in the SSH model given by $\delta(t) = \delta_1$ for $0 < t < 2\pi p_1/\Omega$ and δ_2 for $2\pi p_1/\Omega < t < 2\pi/\Omega$. Here, $0 < p_1 < 1$ is the dimensionless fraction of the period for the first step of the drive. This family of protocols simplifies the numerical calculations, and allows us to obtain both analytically exact and numerically reliable results over a wide range of frequencies. Note that the modulation is chiral symmetric. This is explicit if we take the origin of time to be at $\pi p_1/\Omega$. Calculating the full-period evolution operator, the quasienergies are given by

$$\cos \frac{2\pi\epsilon_k}{\Omega} = \cos \frac{2\pi\bar{E}_k}{\Omega} \cos^2 \frac{\theta_k}{2} + \cos \frac{2\pi\check{E}_k}{\Omega} \sin^2 \frac{\theta_k}{2}, \quad (3)$$

where the average and difference bands $\bar{E}_k = p_1|d_{1k}| + p_2|d_{2k}|$, $\check{E}_k = p_1|d_{1k}| - p_2|d_{2k}|$ with index $a = 1, 2$, indicating $\delta = \delta_a$. Here, θ_k is the angle between the complex variables d_{1k} and d_{2k} . Without loss of generality, we assume $|\delta_1| > |\delta_2|$. Gap closings at ϵ° for $k_*^\circ \neq 0, \pi$ are obtained when $\cos(2\pi\bar{E}_{k_*^\circ}/\Omega) = \cos(2\pi\check{E}_{k_*^\circ}/\Omega) = (-1)^\circ$, where $(-1)^b = -1$ and $(-1)^\natural = 1$. This is a resonant condition leading to an implicit equation for Ω , which we solve numerically. Furthermore, for $|\delta_2/\delta_1|p_2 < p_1 < p_2$,

there exist k_*^\natural where $\check{E}_{k_*^\natural} = 0$; at these points, the gap at ϵ^\natural closes for $\bar{E}_{k_*^\natural}/\Omega_*^\natural \equiv 0 \bmod 1$.

The winding numbers are found from

$$D_k = e^{-i\theta_k/2} \left(\cos \frac{\pi\bar{E}_k}{\Omega} \cos \frac{\theta_k}{2} + i \cos \frac{\pi\check{E}_k}{\Omega} \sin \frac{\theta_k}{2} \right) \quad (4)$$

and $B_k = (d_{1k}/|d_{1k}|)\tilde{B}_k$,

$$\tilde{B}_k = e^{-i\theta_k/2} \left(\sin \frac{\pi\bar{E}_k}{\Omega} \cos \frac{\theta_k}{2} + i \sin \frac{\pi\check{E}_k}{\Omega} \sin \frac{\theta_k}{2} \right). \quad (5)$$

Since $\theta_\pi = 0$ or π and $\theta_0 = 0$, D_π (\tilde{B}_π) and D_0 (\tilde{B}_0) are real. We note $\mathcal{W}[B] = \mathcal{W}[d_1] + \mathcal{W}[\tilde{B}]$, i.e. $\nu^\natural = \nu_1 + \mathcal{W}[\tilde{B}]$.

Focusing on ν^b for concreteness and using the explicit forms of D_k , we find that the crossing points that contribute to either N_+ or N_- are emitted when $2p_1w/\Omega$ or $2p_2w/\Omega$ is an integer, and they are absorbed when $p_1|\delta_1|/\Omega$ or $2p_2|\delta_2|/\Omega$ is an integer. For $p_1 \approx p_2$ and for small enough frequency, we may assume the motion of crossing points yields a nearly uniform distribution along the real axis. Since the winding number varies by 2 only when the crossing two points are on different halves of the real axis, the diffusion constant may be obtained by

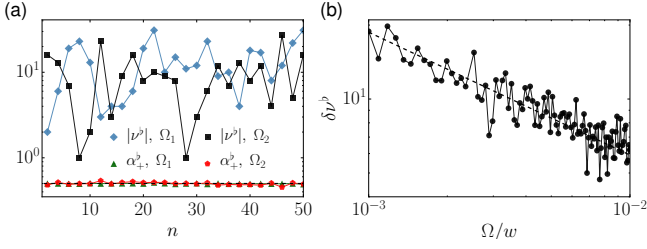


FIG. 3. (color online) (a) Winding number, $|\nu^b|$, and the ratio α_+^b in a multi-step protocol as a function of the number of steps, n . The two frequencies are $\Omega_1/w = 1.09 \times 10^{-3}$ and $\Omega_2/w = 4.15 \times 10^{-3}$, with the mean value $\bar{\delta}/w = -0.4$ and amplitude $A/w = 0.1$. (b) The root-mean-square, $\delta\nu^b$, averaged over n as a function frequency. The dashed line corresponds to $\sqrt{\mathcal{D}^b/\Omega}$, fitted with $\mathcal{D}^b/w = 0.35$.

$\mathcal{D}^b \approx 2|p_1(w - |\delta_1|) - p_2(w - |\delta_2|)|$. In the following, we assume $\delta_1 < 0$ for simplicity.

Our analytical expressions for the two-step drive allow for the exact determination of gap closings; however, in general, quasienergy gaps and topological invariants can only be obtained by numerical solutions. In the special case of a symmetric drive, $\delta_2 = -\delta_1$ and $p_1 = p_2$, we can calculate the topological invariants exactly: $\nu^b = 0$, and $\nu^b = -1$ when $\lfloor \frac{2w}{\Omega} - \frac{1}{2} \rfloor$ is even and 0 otherwise.

For the numerical solutions, we consider three distinct protocols: the *asymmetric protocol*, $\delta_2 = -\delta_1 - \varrho > 0$, which is a periodic switch between the equilibrium trivial and the topological phases with the asymmetry parameter ϱ ; the *critical protocol*, $\delta_2 = 0$, i.e. a periodic switch between the equilibrium trivial and the critical point of the system; and finally, the *trivial protocol*, $\delta_1 < \delta_2 < 0$, such that the systems is in the equilibrium trivial phase at all times. Our numerical results for ν^b are summarized in Fig. 2; our results for ν^b are similar [45].

The quasienergy gaps $\Delta^\circ = \min_k |\epsilon_k - \epsilon^\circ|$ exhibit self-similar patterns, with peaks that scale as $\sim \Omega^2$. We have benchmarked our numerical calculation with the exact analytical expressions for gap closings, shown on the same plot; the agreement is extremely good. The Ω^2 scaling can be understood within adiabatic perturbation theory [50, 51], where the frequency is used as a perturbation parameter. The first-order correction to the quasienergy is the Berry phase of the steady states, which vanishes for our chirally symmetric protocols [51, 52].

The winding number ν^b fluctuates as frequency is lowered with an increasing relative amplitude. For an asymmetric protocol, as in Fig. 2(c) center panel, when $\Omega > 2\varrho$, we observe the regular step-wise behavior as in the symmetric protocol. However, when $\Omega < 2\varrho$, the same fluctuating pattern sets in. We have carried out a detailed analysis of ν^b over a wide range of low frequencies. For each frequency Ω , we show N^b , N_+^b , $\alpha_+^b = N_+^b/N^b$, and ν^b . Both N^b , and N_+^b scale linearly with $1/\Omega$, confirming our general arguments. The ratio α_+^b approaches $1/2$ as the frequency decreases, indicating

the diffusive behavior familiar from a random-walk process. Moreover, the range of $|\nu^b|$ scales as $\sim 1/\sqrt{\Omega}$. For a range of frequencies much lower than other energy scales in the system, we have determine the probability $P(\nu^b)$ of finding ν^b in our numerical histogram. As shown, $P(\nu^b)$ follows a Gaussian distribution with a width that is given by $\sigma(\nu^b) = \sqrt{\mathcal{D}^b/\Omega}$ over several decades of frequency, confirming our general result.

To test our general arguments for the universality of the fluctuations, we have studied other drive protocols and other models, including a model with multiple bands. These numerical studies support our results in all cases. Details are found in the Supplemental Material [45]; here, we present our results for a multi-step protocol in the SSH model approximating $\delta(t) = \bar{\delta} + A \cos(\Omega t)$. The analytical calculations become increasingly difficult as the number of steps n in the drive increases; however, we can still calculate the topological invariants numerically. A typical sampling of our results are shown in Fig. 7. While ν^b fluctuates both in magnitude and sign as n is varied, the ratio $\alpha_+^b \approx 1/2$, again indicating a diffusive process. Collecting good statistics over a wide frequency range quickly becomes too expensive. However, since the fluctuations in the winding number result from the twisting and untwisting of the contour D_k , we expect that varying the number of steps n should have a similar effect. Indeed, as shown in Fig. 7(b), after averaging over n , the root-mean-square $\delta\nu^b \sim 1/\sqrt{\Omega}$.

In conclusion, we have found universal fluctuations in the topological invariants characterizing a Floquet topological phase. We explained these fluctuations by positing a pseudorandom distribution of crossing points of the complex function whose winding number gives the topological invariant. This distribution follows from the diffusive process of emission, absorption, and motion of crossing points as frequency is lowered. Our results show that the limit $\Omega \rightarrow 0$ has a rich structure that is distinct from the simple adiabatic limit: while the topological invariant vanishes [53] on average, consistent with the adiabatic limit, its fluctuations diverge. These fluctuation may be observed in the noise spectra of relevant quantities such as voltage noise [56], or by spectroscopic measures of the number of Floquet edge modes as recently observed in a photonic crystal emulator [25].

Universal fluctuations in Chern numbers have been studied in quantized classically-chaotic and random matrix theories [54, 55]. By contrast, we study periodically driven systems, where topology is characterized not just by Chern numbers of a static Hamiltonian, but by independent winding numbers through a drive cycle. In this context, it would be interesting to study if driven systems with different symmetries (say, other than chiral symmetry) can support other universality classes of fluctuations of Floquet topological invariants.

This work was supported in part by BSF grant No. 2014345, NSF CAREER grant DMR-1350663, and the

College of Arts and Sciences at Indiana University. M.R.V. acknowledges the support and hospitality of Max Planck Institute for the Physics of Complex Systems.

-
- [1] P. Kapitza, Soviet Phys. JETP **21**, 588 (1951).
 - [2] M. J. Feigenbaum, J. Stat. Phys. **19**, 25 (1978).
 - [3] J. Wang and J. Gong Phys. Rev. A **77**, 031405(R) (2008).
 - [4] G. Jotzu, M. Messer, R. Desbuquois, M. Lebrat, T. Uehlinger, D. Greif, and T. Esslinger, Nature **515**, 237 (2014).
 - [5] M. Aidelsburger, M. Lohse, C. Schweizer, M. Atala, J. T. Barreiro, S. Nascimbene, N. R. Cooper, I. Bloch, and N. Goldman, Nat. Phys. **11**, 162 (2015).
 - [6] J. Zhang, P. W. Hess, A. Kyprianidis, P. Becker, A. Lee, J. Smith, G. Pagano, I.-D. Potirniche, A. C. Potter, A. Vishwanath, N. Y. Yao, and C. Monroe, Nature **543**, 217 (2017).
 - [7] S. Choi, J. Choi, R. Landig, G. Kucsko, H. Zhou, J. Isoya, F. Jelezko, S. Onoda, H. Sumiya, V. Khemani, C. v. Keyserlingk, N. Y. Yao, E. Demler, and M. D. Lukin Nature **543**, 221 (2017).
 - [8] A. Eckardt, Rev. Mod. Phys. **89**, 011004 (2017).
 - [9] T. Oka and H. Aoki, Phys. Rev. B **79**, 081406 (2009).
 - [10] T. Kitagawa, T. Oka, A. Brataas, L. Fu, and E. Demler, Phys. Rev. B **84**, 235108 (2011).
 - [11] N. H. Lindner, G. Refael, and V. Galitski, Nat. Phys. **7**, 490 (2011).
 - [12] L. Jiang, T. Kitagawa, J. Alicea, A. R. Akhmerov, D. Pekker, G. Refael, J. I. Cirac, E. Demler, M. D. Lukin, and P. Zoller, Phys. Rev. Lett. **106**, 220402 (2011).
 - [13] Z. Gu, H. A. Fertig, D. P. Arovas, and A. Auerbach, Phys. Rev. Lett. **107**, 216601 (2011).
 - [14] B. Dóra, J. Cayssol, F. Simon, and R. Moessner, Phys. Rev. Lett. **108**, 056602 (2012).
 - [15] A. Kundu and B. Seradjeh, Phys. Rev. Lett. **111**, 136402 (2013).
 - [16] A. Kundu, H. A. Fertig, and B. Seradjeh, Phys. Rev. Lett. **113**, 236803 (2014).
 - [17] P. M. Perez-Piskunow, G. Usaj, C. A. Balseiro, and L. E. F. Foa Torres, Phys. Rev. B **89**, 121401 (2014).
 - [18] L. Zhou, H. Wang, D. Y. H. Ho, J. Gong, Eur. Phys. J. B **87**, 204 (2014).
 - [19] D. Y. H. Ho and J. Gong Phys. Rev. Lett. **109**, 010601 (2012).
 - [20] P. Titum, N. H. Lindner, M. C. Rechtsman, and G. Refael, Phys. Rev. Lett. **114**, 056801 (2015).
 - [21] A. Kundu, H. A. Fertig, and B. Seradjeh, Phys. Rev. Lett. **116**, 016802 (2016).
 - [22] M. C. Rechtsman, J. M. Zeuner, Y. Plotnik, Y. Lumer, D. Podolsky, F. Dreisow, S. Nolte, M. Segev, and A. Szameit, Nature **496**, 196 (2013).
 - [23] Y. H. Wang, H. Steinberg, P. Jarillo-Herrero, and N. Gedik, Science **342**, 453 (2013).
 - [24] E. J. Sie, C. H. Lui, Y.-H. Lee, L. Fu, J. Kong, and N. Gedik, Science **355**, 1066 (2017).
 - [25] Q. Cheng, Y. Pan, H. Wang, C. Zhang, D. Yu, A. Gover, H. Zhang, T. Li, L. Zhou, and S. Zhu, arXiv:1804.05134.
 - [26] S. Blanes, F. Casas, J. Oteo, and J. Ros, Phys. Rep. **470**, 151 (2009).
 - [27] S. Rahav, I. Gilary, and S. Fishman, Phys. Rev. A **68**, 013820 (2003).
 - [28] S. Rahav, I. Gilary, and S. Fishman, Phys. Rev. Lett. **91**, 110404 (2003).
 - [29] M. Bukov, L. D'Alessio, and A. Polkovnikov, Adv. Phys. **64**, 139 (2015).
 - [30] A. Eckardt and E. Anisimovas, N. J. Phys. **17**, 093039 (2015).
 - [31] T. Mikami, S. Kitamura, K. Yasuda, N. Tsuji, T. Oka, and H. Aoki, Phys. Rev. B **93**, 144307 (2016).
 - [32] A. Gómez-León and G. Platero, Phys. Rev. Lett. **110**, 200403 (2013).
 - [33] A. Lazarides, A. Das, and R. Moessner, Phys. Rev. E **90**, 012110 (2014).
 - [34] L. D'Alessio and M. Rigol, Phys. Rev. X **4**, 041048 (2014).
 - [35] S. A. Weidinger and M. Knap, Sci. Rep. **7**, 45382 (2017).
 - [36] C. Sträter and A. Eckardt, Z. Naturforsch. A **71**, 909 (2016).
 - [37] D. E. Liu, A. Levchenko, and H. U. Baranger, Phys. Rev. Lett. **111**, 047002 (2013).
 - [38] Q.-J. Tong, J.-H. An, J. Gong, H.-G. Luo, and C. H. Oh, Phys. Rev. B **87**, 201109 (2013).
 - [39] Á. Gómez-León, P. Delplace, and G. Platero, Phys. Rev. B **89**, 205408 (2014).
 - [40] T. Mikami, S. Kitamura, K. Yasuda, N. Tsuji, T. Oka, and H. Aoki, Phys. Rev. B **93**, 144307 (2016).
 - [41] D. Y. H. Ho and J. Gong, Phys. Rev. B **90**, 195419 (2014).
 - [42] J. K. Asbóth, B. Tarasinski, and P. Delplace, Phys. Rev. B **90**, 125143 (2014).
 - [43] V. Dal Lago, M. Atala, and L. E. F. Foa Torres, Phys. Rev. A **92**, 023624 (2015).
 - [44] W. P. Su, J. R. Schrieffer, and A. J. Heeger, Phys. Rev. Lett. **42**, 1698 (1979).
 - [45] See Supplemental Material, where additional information is provided for the SSH, Kitaev, and SSH-Kitaev models with open and periodic boundary conditions.
 - [46] A. Yu. Kitaev, Phys.-Usp. **44**, 131 (2001).
 - [47] R. Wakatsuki, M. Ezawa, Y. Tanaka, and N. Nagaosa, Phys. Rev. B **90**, 014505 (2014).
 - [48] We use this “musical notation,” instead of the more common “0” and “ π ,” to avoid confusion with crystal momenta at $k = 0$ and $k = \pi$.
 - [49] Exceptions from this universal process may occur for fine-tuned drive protocols, for example the symmetric two-step drive in the SSH model discussed later.
 - [50] G. Rigolin, G. Ortiz, and V. H. Ponce, Phys. Rev. A **78**, 052508 (2008).
 - [51] M. Rodriguez-Vega, M. Lentz, and B. Seradjeh, arXiv:1805.01190.
 - [52] H. Martiskainen and N. Moiseyev, Phys. Rev. A **91**, 023416 (2015).
 - [53] Note that the average may also be a small nonzero number, as for ν^b in the asymmetric protocol shown in Fig. 3(c), center panel. An example for ν^b is when the drive protocol is entirely in the equilibrium topological phase.
 - [54] P. Leboeuf, J. Kurchan, M. Feingold, and D. P. Arovas, Phys. Rev. Lett. **65**, 3076 (1990).
 - [55] P. N. Walker and M. Wilkinson, Phys. Rev. Lett. **74**, 4055 (1995).
 - [56] M. Rodriguez-Vega, H. A. Fertig, and B. Seradjeh, arXiv:1803.10646.

SUPPLEMENTAL MATERIAL

In this Supplemental Material, we recap, for completeness, the derivation of the Floquet topological invariants in one-dimensional driven systems with a chiral reflection symmetry, and present the details of our numerical studies for driven Su-Schrieffer-Heeger (SSH), Kitaev, and SSH-Kitaev models, as well as the multi-step drive protocol in driven SSH model.

Topological invariant for driven one-dimensional chiral-symmetric systems

In this section, we briefly outline the derivation of the topological invariant for one-dimensional chiral symmetric systems, following Ref. [1]. A driven system has chiral symmetry if there exist a unitary, hermitian, local operator $\Gamma = \Gamma^\dagger = \Gamma^{-1}$, such that

$$\Gamma U(\tau, \tau + T) \Gamma = U^{-1}(\tau, \tau + T) \quad (6)$$

where the time-ordered exponential $U(\tau, \tau + T) = \mathbb{T} \exp \left[-i\hbar \int_\tau^{\tau+T} H(s) ds \right]$ is the full-period evolution operator with the initial time τ and period $T = 2\pi/\Omega$ for the Hamiltonian $H(t) = H(t + T)$. A topological invariant characterizing a chiral-symmetric one-dimensional system with periodic boundary conditions can be written in the diagonal basis of Γ , where

$$H_{\text{eff}}(\tau) \equiv \frac{i}{T} \ln U(\tau, \tau + T) = \begin{bmatrix} 0 & h(\tau) \\ h^\dagger(\tau) & 0 \end{bmatrix}, \quad (7)$$

as

$$\nu_\tau = \mathcal{W}[h(\tau)] = \frac{1}{2\pi i} \int_{-\pi}^{\pi} dk \frac{\partial}{\partial k} \ln[\det h_k(\tau)]. \quad (8)$$

where k is the lattice momentum.

Now, we say the drive protocol in $H(t)$ has chiral reflection symmetry if for some τ and $\tau' \in (0, T)$, one has $U(\tau + \tau', \tau + T) = \Gamma F^\dagger \Gamma$, where $F = U(\tau, \tau + \tau')$. That is, the drive protocol starting at τ has a reflection symmetry about $\tau + \tau'$. Then, $U(\tau, \tau + T) = \Gamma F^\dagger \Gamma F$ and $U(\tau + \tau', \tau + \tau' + T) = F \Gamma F^\dagger \Gamma$ both satisfy Eq. (6).

Thus, we can define two topological invariants $\nu = \nu_\tau$ and $\nu' = \nu_{\tau+\tau'}$. Physically, they can be interpreted as a bulk “sublattice” polarization at times τ , and $\tau + \tau'$. Given that states with quasienergy $\epsilon^b = \Omega/2$ switch sublattice when they evolve from τ to $\tau + \tau'$, neither ν nor ν' alone are related to the number of edge states in an open system, instead

$$\nu^{\natural} = \frac{1}{2} (\nu + \nu'), \quad \nu^b = \frac{1}{2} (\nu - \nu'), \quad (9)$$

where ν^{\natural} and ν^b are the number of edge states with quasienergy $\epsilon^{\natural} = 0$, and $\epsilon^b = \Omega/2$, respectively. Using algebraic properties of winding numbers in the diagonal basis of Γ , the authors of Ref. [1] showed that ν^{\natural} and ν^b can be derived from the diagonal and off-diagonal blocks of $F = \begin{bmatrix} A & B \\ C & D \end{bmatrix}$ as $\nu^{\natural} = \mathcal{W}[B]$, $\nu^b = \mathcal{W}[D]$.

Driven SSH model

The tight-binding Hamiltonian for driven the Su-Schrieffer-Heeger (SSH) model is given by the

$$\hat{H}(t) = \sum_r [w + (-1)^r \delta(t)] \hat{c}_{r+1}^\dagger \hat{c}_r + \text{h.c.}, \quad (10)$$

where \hat{c}_r^\dagger creates a fermion at lattice site r , w is the unmodulated hopping amplitude and $\delta(t) = \delta(t + 2\pi/\Omega)$ is the hopping modulation, periodic in time with frequency Ω . For periodic boundary conditions, the crystal momentum k is a good quantum number; defining the spinor $\hat{c}_k^\dagger = \sum_x e^{ikx} (\hat{c}_{2x}^\dagger, \hat{c}_{2x+1}^\dagger)$, where $x = \lfloor r/2 \rfloor$ indexes the unit cells, we have $\hat{H} = \int \hat{c}_k^\dagger h_k \hat{c}_k \frac{dk}{2\pi}$, with k in the Brillouin zone $[-\pi, \pi]$, $h_k = d_{kx} \sigma_x + d_{ky} \sigma_y$ and $d_{kx} + id_{ky} \equiv d_k = 2e^{ik/2} (w \cos \frac{k}{2} + i\delta \sin \frac{k}{2})$. Discrete symmetries of this Hamiltonian include inversion $\sigma_x h_k \sigma_x = h_{-k}$, sublattice $\sigma_z h_k \sigma_z = -h_k$, and particle-hole symmetry $\sigma_y h_k^* \sigma_y = -h_k$, which place the static SSH model in the BDI class [2]. The instantaneous eigenvalues are $\pm |d_k|$ with $|d_k| = 2\sqrt{w^2 \cos^2 \frac{k}{2} + \delta^2 \sin^2 \frac{k}{2}}$.

Quasienergy spectrum

In this section, we consider a driven SSH model with open boundary conditions, and calculate the number of edge states present in the system at given frequency. Fig. 4 shows the quasienergies as a function of the inverse frequency in the range $\Omega/w \in [0.1, 1]$. The system has $N = 1000$ sites and is driven by a two-step protocol switching between $\delta_1/w = -0.75$ and $\delta_2/w = -0.25$. States with quasienergies $\epsilon^b = 0$, and $\epsilon^b = \Omega/2$ are localized at the edge of the system.

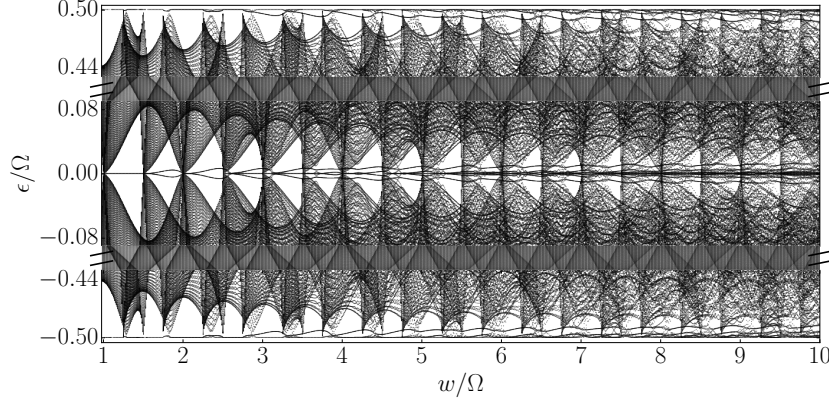


FIG. 4. Quasienergy spectrum of the driven SSH model with open boundary conditions as a function of inverse frequency. The chain has 1000 sites and is subject to a two-step drive protocol switching between $\delta_1/w = -0.75$ and $\delta_2/w = -0.25$. Edge states within quasienergy gaps at $\epsilon^b = 0$ and $\epsilon^b = \Omega/2$ are found in an increasing number as the frequency is lowered.

Top panel of Fig. 5(a) [(b)] shows n^b (n^a), the number of edge mode pairs with quasienergies ϵ^b (ϵ^a), and are compared with the corresponding topological invariant ν^b (ν^a). We use the same parameters as in Fig. 4. In order to correctly resolve the quasienergies, we consider a systems with $N = 1000$ sites for the range $w/\Omega \in [0.3, 1]$, $N = 2000$ for $w/\Omega \in [1, 3]$, and $N = 3000$ for $w/\Omega \in [3, 3.38]$.

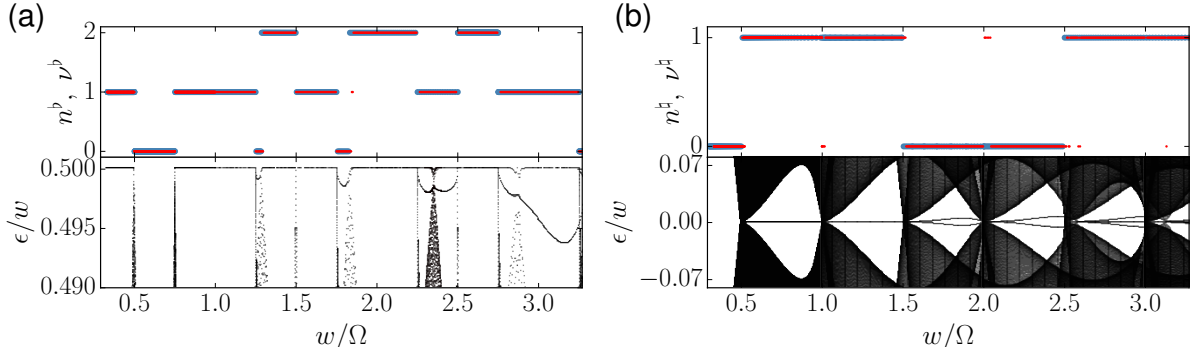


FIG. 5. (a) Top: number of edge states n^b (red) with quasienergy $\epsilon^b = \Omega/2$ on top of the invariant ν^b (blue) as a function of inverse frequency. Bottom: quasienergy spectrum around $\epsilon^b = \Omega/2$. (b) Top: same as (a) for n^a (red) and ν^a (blue). Bottom: quasienergy spectrum around $\epsilon^a = 0$. All the parameters are same as in Fig. 4.

Both quantities are in agreement, as expected from the bulk-boundary correspondence. Deviations are observed at frequencies in proximity to gap closings, where a larger system is required to correctly resolve the spectrum. Bottom panel of Fig. 5(a) [(b)] shows a close-up in the quasienergy spectrum around ϵ^b (ϵ^a). Changes in ν^b (ν^a) occur only when the gap around ϵ^b (ϵ^a) closes.

Topological invariant ν^{\natural}

In this section, we discuss the low-frequency limit of ν^{\natural} , the topological invariant related to the number of edge states with quasienergy ϵ^{\natural} . As discussed in the main text, ν^{\natural} also presents fluctuations in the low-frequency regime, with exceptions in special cases. For example, in the case of a symmetric drive, with $\delta_2 = -\delta_1$ and $p_1 = p_2$ we obtain $\nu^{\natural} = 0$.

In general, we have to evaluate the invariant ν^{\natural} numerically. Fig. 6 summarizes our results. The winding number ν^{\natural} fluctuates as frequency is lowered with a relative amplitude that grows as $\Omega \rightarrow 0$. Both N^{\natural} and N_+^{\natural} scale linearly with $1/\Omega$. The ratio $\alpha_+^{\natural} = N_+^{\natural}/N^{\natural}$ approaches $1/2$ as the frequency decreases. Moreover, the range of $|\nu^{\natural}|$ scales as $\sim 1/\sqrt{\Omega}$. All of these properties are similar to the low-frequency behavior of ν^b . For a range of frequencies much lower than other energy scales in the system, we have determined the probability $P(\nu^{\natural})$ of finding ν^{\natural} in our numerical histogram. As shown, $P(\nu^{\natural})$ follows a Gaussian distribution with a width that is given by $\sigma(\nu^{\natural}) = \sqrt{\mathcal{D}^{\natural}/\Omega}$ over a decade of frequencies. When the drive protocol is entirely in the static topological (trivial) phase, the probability $P(\nu^{\natural})$ is centered at $\nu^{\natural} = 1$ ($\nu^{\natural} = 0$).

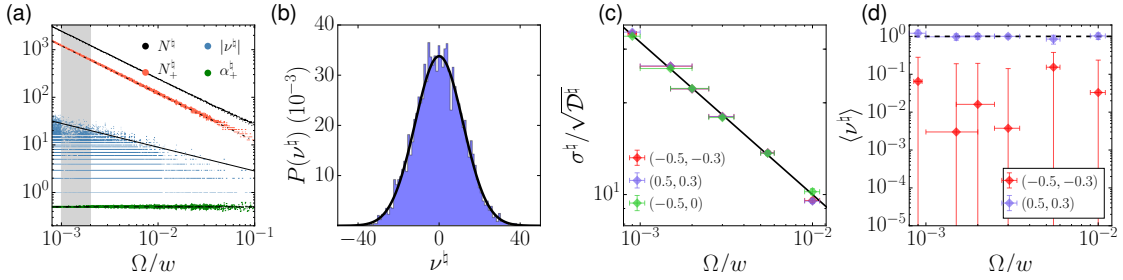


FIG. 6. (a) Statistics of crossing points and winding number for a trivial protocol with $(\delta_1/w, \delta_2/w) = (-0.5, -0.3)$. From top to bottom: the total number of crossing points, N^{\natural} , the positively-oriented crossing points N_+^{\natural} , the ratio $\alpha_+^{\natural} = N_+^{\natural}/N^{\natural}$, and the winding number $|\nu^{\natural}|$ are calculated numerically at 30000 frequencies. The solid line shows $\sqrt{\mathcal{D}^{\natural}}/\Omega$ with $\mathcal{D}^{\natural} = ||\delta_1| - |\delta_2||$. (b) Probability distribution of ν^{\natural} for the trivial protocol in (a) and frequency range $\Omega/w \in (1, 2) \times 10^{-3}$. The solid line is a Gaussian fit. (c) Standard deviation $\sigma^{\natural}(\Omega)$ for various two-step drive protocols found by a Gaussian fit to $P(\nu^{\natural})$. The horizontal (vertical) line at each point indicates the range of frequencies (fitting error). The legend shows the values $(\delta_1/w, \delta_2/w)$. The solid line is $\sigma^{\natural} = \sqrt{\mathcal{D}^{\natural}}/\Omega$. (d) Average $\langle \nu^{\natural} \rangle$, found by a Gaussian fit to $P(\nu^{\natural})$.

Multi-step drive protocol

In this section, we consider a multi-step driving protocol as an approximation to the smooth protocol $\delta(t) = \bar{\delta} + A \cos(\Omega t)$. For a protocol with n steps, the half-propagator is given by

$$U_k(\pi/\Omega) = \prod_{j=0}^n e^{-i h_k(j\pi/(\Omega n))\pi/(\Omega n)}. \quad (11)$$

In the limit $n \rightarrow \infty$ we recover the smooth protocol. In Fig. 7(a) we plot the invariant $|\nu^b|$ and the ratio α_+^b as a function of the frequency Ω for a protocol with $n = 20$ steps. As in the case of a two-step drive, we find that the ratio α_+^b approaches $1/2$ as the frequency decreases, suggesting a diffusive process. Also, $|\nu^b|$ presents fluctuations that grow as $\sim 1/\sqrt{\Omega}$. For large n , it becomes difficult to accurately calculate the invariant, and collecting enough statistics as a function of frequency to determine the scaling in the low-frequency limit becomes more challenging. However, varying n changes the structure of complex function D_k , creating new twists. Therefore, we compute ν^b for different frequencies Ω as a function of n in the range $[2, 50]$ and consider the average over n . In Fig. 7(b), we plot the root-mean-square $\delta\nu^b$ as a function of frequency and find that it also scales as $1/\sqrt{\Omega}$.

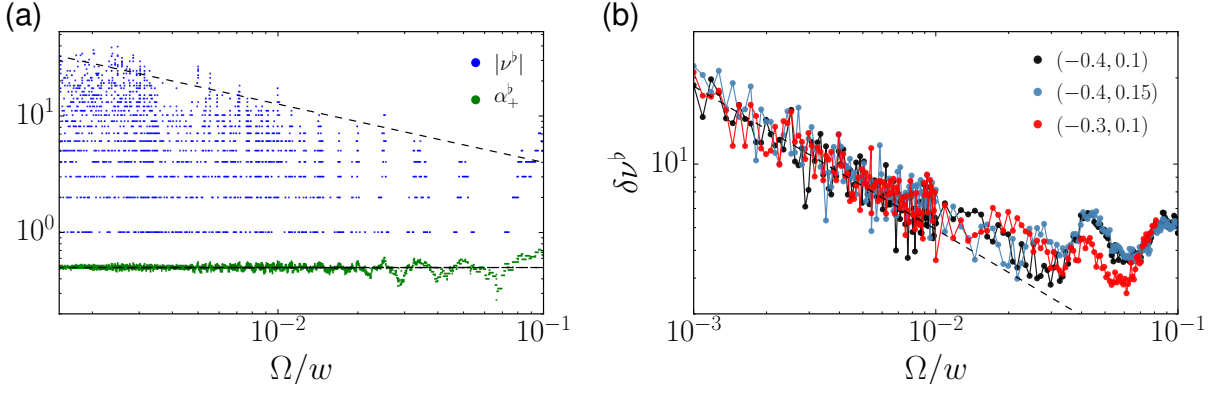


FIG. 7. (a) Winding number, $|\nu^b|$, and the ratio α_+^b in a multi-step protocol as a function of the frequency Ω . The number of steps in the drive is $n = 20$ with the mean value $\bar{\delta}/w = -0.4$ and amplitude $A/w = 0.1$. From top to bottom, the dashed lines correspond to $\sqrt{0.35/\Omega}$ and $1/2$. (b) The root-mean-square $\delta\nu^b$, averaged over n as a function frequency for three sets of $(A, \bar{\delta})$. The dashed line corresponds to $\sqrt{\mathcal{D}^b/\Omega}$, fitted with $\mathcal{D}^b/w = 0.5$.

Driven Kitaev Model

In this section we consider the driven Kitaev model, and study the behaviour of the topological invariants in the low-frequency regime. The Hamiltonian is given by [3]

$$\hat{H} = \sum_{r=1}^{N-1} \left(w \hat{c}_{r+1}^\dagger \hat{c}_r + \Delta \hat{c}_{r+1}^\dagger \hat{c}_r^\dagger + h.c. \right) - \mu \sum_{r=1}^N \hat{c}_r^\dagger \hat{c}_r, \quad (12)$$

where w and Δ are the nearest-neighbor hopping and pairing amplitudes respectively, and μ is the chemical potential. Imposing periodic boundary conditions, and introducing the Nambu spinors $\hat{\psi}_k^\top = (\hat{c}_k, \hat{c}_{-k}^\dagger)$, the Hamiltonian can be written as $\hat{H} = \frac{1}{2} \sum_k \hat{\psi}_k^\dagger h_k \hat{\psi}_k - \mu N$, where $h_k = (2w \cos k - \mu) \sigma_z + 2|\Delta| \sin k (\cos \phi \sigma_y - \sin \phi \sigma_x)$. This has the particle-hole symmetry $h_k = -\sigma_x h_{-k}^* \sigma_x$. Upon the rotation $R = \exp(-i\sigma_y \pi/4) \exp(i\phi \sigma_z/2)$, the Hamiltonian is transformed to

$$h_k \rightarrow R h_k R^\dagger = (2w \cos k - \mu) \sigma_x + |\Delta| \sin k \sigma_y, \quad (13)$$

as shown in the main text. In this representation, the Kitaev model has the discrete symmetries $h_k = -\sigma_z h_{-k}^* \sigma_z$, and $h_k = h_{-k}^*$. The instantaneous eigenvalues are $\pm \sqrt{(2w \cos k - \mu)^2 + |\Delta|^2 \sin^2 k}$.

In a system with open boundary conditions we find one pair of Majorana states at zero energy for $|\mu| < 2|w|$, and zero for $|\mu| > 2|w|$. At $|\mu| = 2w$ the gap closes. The static topological invariant gives $\nu = 1$ for $|\mu| < 2w$ and zero otherwise.

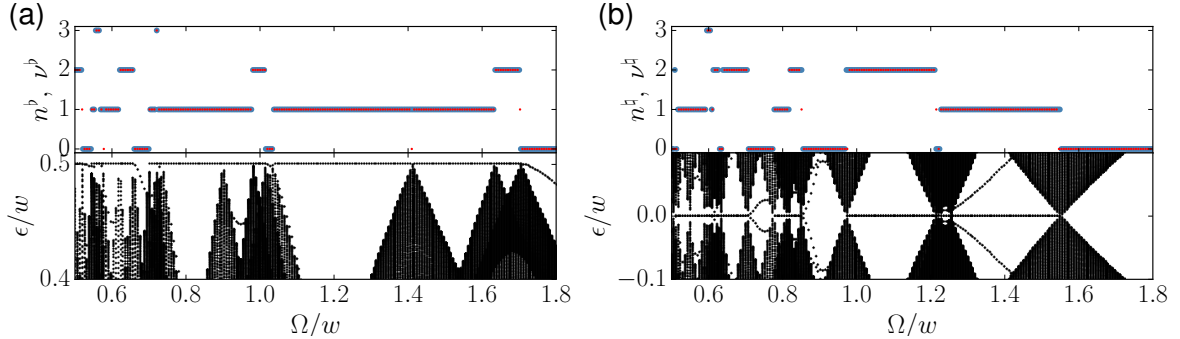


FIG. 8. (a) Top: number of edge states n^b (red) with quasienergy $\epsilon^b = \Omega/2$ on top of the invariant ν^b (blue) as a function of frequency. Bottom: quasienergy spectrum around $\epsilon^b = \Omega/2$ for a system with open boundary conditions and $N = 1000$ sites. (b) Top: same as (a) for n^b (red) and ν^b (blue). Bottom: quasienergy spectrum around $\epsilon^b = 0$. The driving protocol is $(\mu_1/w = 1.0, \mu_2/w = -1.9)$, and $|\Delta|/w = 1$.

Choosing a suitable driving protocol, the driven Kitaev model also has chiral symmetry, and the topological invariants are given by ν^b and ν^\dagger , as for the SSH model. In this work, we choose to drive the chemical potential $\mu(t)$ with the two-step protocol $\mu(t) = \mu_1$ for $0 < t < 2\pi p_1/\Omega$ and μ_2 for $2\pi p_1/\Omega < t < 2\pi/\Omega$, where $0 < p_1 < 1$. We fix $p_1 = 0.5$. The bottom panels in figure 8 show the quasienergy spectrum for a chain with $N = 1000$ sites in the frequency range $\Omega/w \in [0.5, 1.8]$ around the Floquet zone edge and center. Top panel (a) [(b)] shows the topological invariant ν^b (ν^\dagger) underneath the number of states with quasienergy ϵ^b (ϵ^\dagger), shown in red. These quantities are in agreement. Differences can be found at frequencies where the corresponding quasienergy gap is closed.

We now evaluate the topological invariants numerically in the low-frequency regime. For concreteness, we focus on ν^b . Our results are summarized in Fig. 9. As for the SSH model, we find that the range of $|\nu^b|$ scales as $\sim 1/\sqrt{\Omega}$, both N^b and N_+^b scale linearly with $1/\Omega$, and the ratio α_+^b approaches $1/2$ as the frequency decreases. Furthermore, the probability $P(\nu^b)$ follows a Gaussian distribution with width $\sigma(\nu^b) = \sqrt{D^b/\Omega}$.

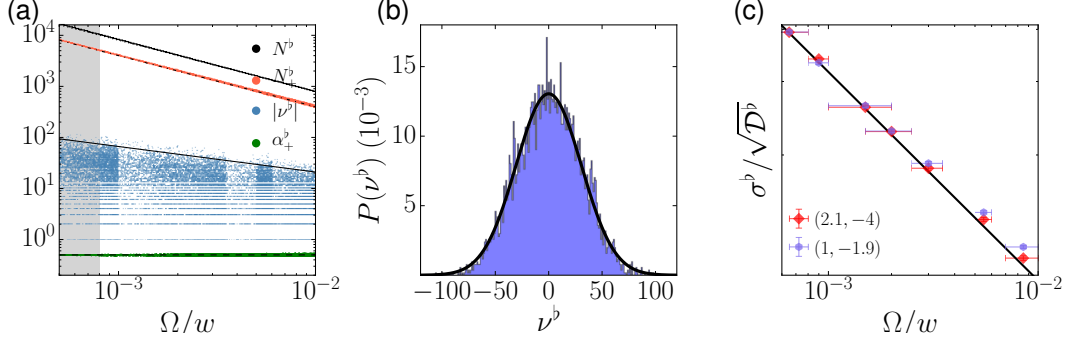


FIG. 9. Topological invariant for a driven Kitaev chain. (a) N^b , N_+^b , $\alpha_+^b = N_+^b/N^b$, and ν^b as a function of the frequency for protocol alternating the chemical potential between $\mu_1/w = 2.1$ and $\mu_2/w = -4$. In panel (b) we plot the probability to obtain ν^b in the range of frequencies shown shaded in (a). (c) shows the width of the Gaussian distribution as a function of frequency for two sets of chemical potentials $(\mu_1/w, \mu_2/w)$. The diffusion constants are $D^b = 0.81$ and $D^b = 0.62$ for $(2.1, -4)$, and $(1, -1.9)$ respectively. The vertical lines indicate the range of frequencies used to calculate the distribution, and the horizontal lines indicate the fitting error. The superconducting gap is fixed in the protocol at $|\Delta|/w = 1$. For each point shown, we considered 5000 frequencies.

Four-band driven Kitaev-SSH Model

In this section we consider the Kitaev-SSH model [4]. The Hamiltonian is given by

$$H = - \sum_x \left\{ w \left[(1 + \delta/w) \hat{c}_{B,x}^\dagger \hat{c}_{A,x} + (1 - \delta/w) \hat{c}_{A,x+1}^\dagger \hat{c}_{B,x} \right] - \Delta \left[(1 + \delta/w) \hat{c}_{B,x}^\dagger \hat{c}_{A,x} + (1 - \delta/w) \hat{c}_{A,x+1}^\dagger \hat{c}_{B,x} \right] - \frac{\mu}{2} \left(\hat{c}_{A,x}^\dagger \hat{c}_{A,x} + \hat{c}_{B,x}^\dagger \hat{c}_{B,x} \right) \right\} + \text{h.c.}, \quad (14)$$

where x labels the unit cells, and A, B label the sublattices in each unit cell, $w + \delta$ ($w - \delta$) and Δ are the intra-cell (inter-cell) hopping and pairing amplitudes respectively and μ is the chemical potential. If we consider periodic boundary conditions, and define the spinor $\hat{\psi}_k^\dagger = (\hat{c}_{kA}^\dagger, \hat{c}_{kB}^\dagger, \hat{c}_{-kA}, \hat{c}_{-kB})$, the momentum-dependent Hamiltonian takes the form [4]

$$h_k = \begin{bmatrix} -\mu & z_k & 0 & \Delta_k \\ z_k^* & -\mu & -\Delta_k^* & 0 \\ 0 & -\Delta_k & \mu & -z_k \\ \Delta_k^* & 0 & -z_k^* & \mu \end{bmatrix}, \quad (15)$$

where $z_k = -[(w + \delta) + (w - \delta)e^{-ik}]$, and $\Delta_k = -\Delta[(1 + \delta/w) - (1 - \delta/w)e^{-ik}]$. For our purpose, the most important feature of this model is that it has four energy bands, given by $\pm \sqrt{\mu^2 + |z_k|^2 + |\Delta_k|^2 \pm 2\sqrt{\mu^2 + |z_k|^2 + (4\Delta\delta)^2}}$.

For $\delta/w < -0.2$ we have two pairs of zero-energy states localized at the edge, while for $-0.2 < \delta/w < 0.2$ we have only one pair. For $\delta/w > 0.2$ there are no zero-energy states. For simplicity, now on we consider the case

$\mu_1/w = \mu_2/w = 0$, although it is possible to also consider finite chemical potentials. The chiral basis for this model is defined by the transformation $\Gamma = \frac{1}{2}(\tau_0 \otimes \sigma_0 + \tau_x \otimes \sigma_x)$, where σ_α and τ_α for $\alpha = x, y, z$ are the Pauli matrices in particle-hole and sublattice space, and $\tau_0 = \sigma_0 = \mathbb{1}$.

We choose the driving protocol $\delta(t) = \delta_1$ for $0 < t < 2\pi p_1/\Omega$ and δ_2 for $2\pi p_1/\Omega < t < 2\pi/\Omega$, where $0 < p_1 < 1$ to ensure that the driven system possesses chiral symmetry. As before, we will fix $p_1 = 0.5$. In Fig. 10, the bottom panels show the quasienergy spectrum for a driven chain with $N = 1000$ sites around the Floquet zone edge (a) and center (b). The rest of the parameters used are $\delta_1/w = 3.0$, $\delta_2/w = -2.0$, and $|\Delta|/w = 0.2$. Top panel (a) [(b)] shows the topological invariant ν^b (ν^h) underneath of n^b (n^h), the number of states with quasienergy $\epsilon^b = \Omega/2$ ($\epsilon^h = 0$), shown in red. These quantities are in agreement, as expected from the bulk-edge correspondence.

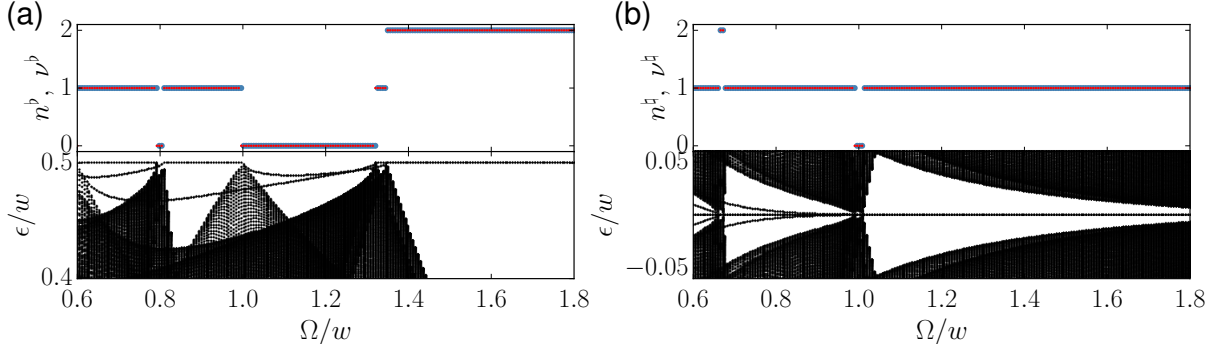


FIG. 10. Top panel: (a) [(b)] Number of edge states n^b (n^h) with quasienergy ϵ^b (ϵ^h), and topological invariant ν^b (ν^h) as a function of frequency. Bottom panel: Quasienergy spectrum as a function of Ω for a driven Kitaev-SSH chain with open boundary conditions. The system has $N = 1000$ sites, $\Delta/w = 0.2$, and the driving protocol ($\delta_1/w = 3.0$, $\delta_2/w = -2.0$).

The topological invariants are derived from the half-period evolution propagator $U_k(\pi/\Omega) \equiv \begin{pmatrix} A_k & B_k \\ C_k & D_k \end{pmatrix}$, where A_k, B_k, C_k and D_k are now 2×2 matrices. The winding numbers are given by $\nu^b = \mathcal{W}[D]$, and $\nu^h = \mathcal{W}[B]$ where $\mathcal{W}[h] = \frac{1}{2\pi i} \int_{-\pi}^{\pi} \frac{\partial}{\partial k} \ln(\det h_k) dk$. As explained in the main text, for multi-band systems, the invariant is still defined by the winding of a complex functions, $\det D_k$ and $\det B_k$. The evaluation of ν^b is done numerically, and our results are summarized in Fig. 11. As in the other two driven chiral-symmetric systems, the SSH model and the Kitaev model, we find that ν^b fluctuates as frequency is lowered. The probability $P(\nu^b)$ also follows a Gaussian distribution, with a width given by $\sigma(\nu^b) = \sqrt{\mathcal{D}^b}/\Omega$.

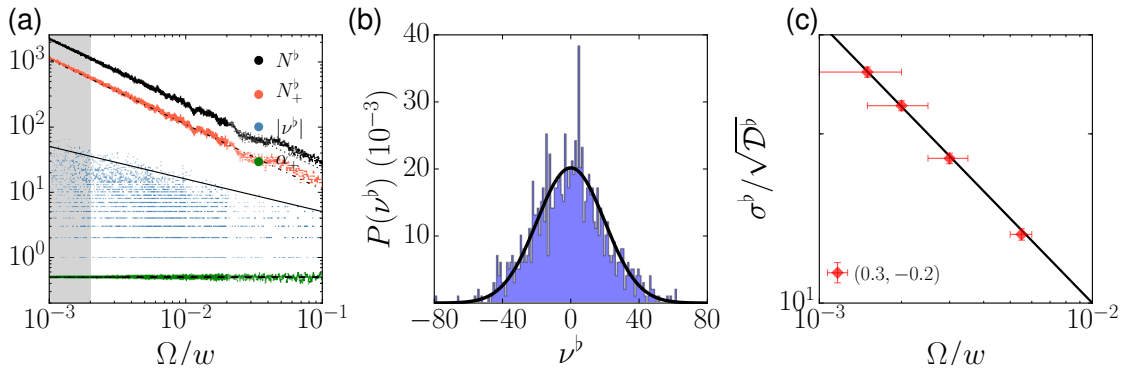


FIG. 11. Topological invariant for a driven Kitaev-SSH chain. (a) N^b , N^b_+ , $\alpha^b_+ = N_+/N$, and ν^b as a function of the frequency. In panel (b) we plot the probability to obtain ν^b in the range of frequencies shown shaded un subpanel (b). Panel (c) shows the width of the Gaussian distribution as a function of frequency for ($\delta_1 = 0.3, \delta_2 = -0.2$). The diffusion constant is $D^b = 0.59$. The vertical lines indicate the range of frequencies used to calculate the distribution, and the horizontal lines indicate the fitting error. The superconducting gap is fixed in the protocol at $|\Delta|/w = 0.2$. For each point shown, we considered 1000 frequencies.

-
- [1] J. K. Asbóth, B. Tarasinski, and P. Delplace, Phys. Rev. B **90**, 125143 (2014).
 - [2] C.-K. Chiu, J. C. Y. Teo, A. P. Schnyder, and S. Ryu, Rev. Mod. Phys. **88** (2016).
 - [3] A. Y. Kitaev, Physics-Uspekhi **44**, 131 (2001).
 - [4] R. Wakatsuki, M. Ezawa, Y. Tanaka, and N. Nagaosa, Phys. Rev. B **90**, 014505 (2014).